Bifurcation analysis of mode-locking structure in a Hodgkin-Huxley neuron under sinusoidal current

Sang-Gui Lee and Seunghwan Kim
Brain Research Center & Nonlinear and Complex Systems Laboratory, Department of Physics, National Core Research Center for System Bio-Dynamics, Pohang University of Science & Technology, San 31 Hyojadong, Pohang, Korea 790-784

(Received 21 September 2004; revised manuscript received 5 December 2005; published 25 April 2006)

Nervous systems under periodic stimuli display rich dynamical states including mode-locking and chaotic responses, which have been a subject of intense studies in neurodynamics. The bifurcation structure of the Hodgkin-Huxley neuron under sinusoidal stimulus is studied in detail. The mechanisms of the firing onset and rich firing dynamics are studied with the help of the codimension-2 bifurcations, which play the role of the organizing center for myriads of saddle-node, period-doubling, and inverse-flip bifurcations forming the boundaries of the complex mode-locking structure. This study provides a useful insight into the organization of similar bifurcation structures in excitable systems such as neurons under periodic forcing.

DOI: 10.1103/PhysRevE.73.041924 PACS number(s): 87.19.La, 05.45.Xt

I. INTRODUCTION

Dynamical systems with two competing frequencies are ubiquitous in nature. Examples include forced mechanical pendula, Belousov-Zhabotinski reactions, and Rayleigh-Benard convections [1]. Rich dynamical states including mode-locking and quasiperiodic states have been extensively studied in these systems involving two competing frequencies [2]. A neuron under periodic stimulus also serves as an important nonlinear dynamical system with two competing frequencies: the natural frequency of the neuron and the external forcing frequency. From the nonlinear interaction between these two frequencies, neurons under periodic stimulus can also exhibit complex dynamical responses including mode locking, quasiperiodicity, and chaos, which have been analyzed with the help of well-developed techniques of nonlinear dynamics [3–6].

The bifurcation analysis of the neuron under periodic stimuli has recently received much attention in connection with various dynamical phenomena including stochastic resonance [7–10] and neuroinformation processing [11–14]. The relationship between the stochastic resonance and deterministic bifurcating structure of mode locking has been studied in diverse ways, and the role of onset bifurcations has been discussed in the context of optimal noise intensity [7–10]. In neurosignal processing, it was recently suggested that the sensory information may also be encoded by temporal patterns of the neural activity [15]. Diverse temporal firing patterns including mode-locking dynamics have been studied in the context of neural information coding. For example, the relationship between bifurcations in Lyapunov exponents and the reliability of neural information has been actively investigated in the context of neurosignal processing [11–14].

Rich dynamical responses in the squid giant axon and the Hodgkin-Huxley neuron model have long served as a paradigm for the nervous system under periodic stimuli [3–5,16]. Well-controlled experiments have been performed for the squid giant axon under external periodic stimuli [3–5]. In these experiments, a periodic pulse current was injected into the squid giant axon in natural sea water [4,5] or a sinusoidal current was injected to the squid giant axon in calcium deficient water [3]. Rich dynamical states including mode-locking, quasiperiodicity, and intermittency routes to chaos were investigated in these systems. These dynamical states have been investigated numerically for the Hodgkin-Huxley neuron under periodic stimuli [6]. These studies led to the complex mode-locking structure of firing dynamics involving various bifurcations including inverse flip, period doubling, and saddle-node bifurcations.

In spite of the wealth of the studies on firing dynamics and associated bifurcations of the neurons, it was not well understood how myriads of bifurcations are organized to form the complex mode-locking structure. In particular, the bifurcation structures near the firing onset are very complicated, which leads to diverse firing onset mechanisms depending on the parameters of the neuron. In this paper, we obtain the detailed picture of the organization of cluster of bifurcation curves near the firing onset. These bifurcations are computed numerically exactly with the help of continuation algorithms [17,18]. We find that three types of codimension-2 bifurcation points organize the cluster of bifurcation curves near the firing onset. A cusp singularity organizes two saddle-node bifurcation curves. Another codimension-2 bifurcation point organizes the period-doubling, inverse-flip, and saddle-node bifurcations. The third codimension-2 bifurcation point organizes the period-doubling, saddle-node, and Hopf bifurcations. These three types of codimension-2 bifurcation points provide a fundamental description of common bifurcation structures near the firing onset of the Hodgkin-Huxley neuron under sinusoidal current.

This study is expected to provide a useful insight into similar bifurcation structures in other excitable systems of neurons under periodic forcing. Recent theoretical studies such as the bifurcation analysis focused on integrate-and-fire neurons, which is the simplest neuron model with spiking nature, and the relaxation oscillators [19] and in the

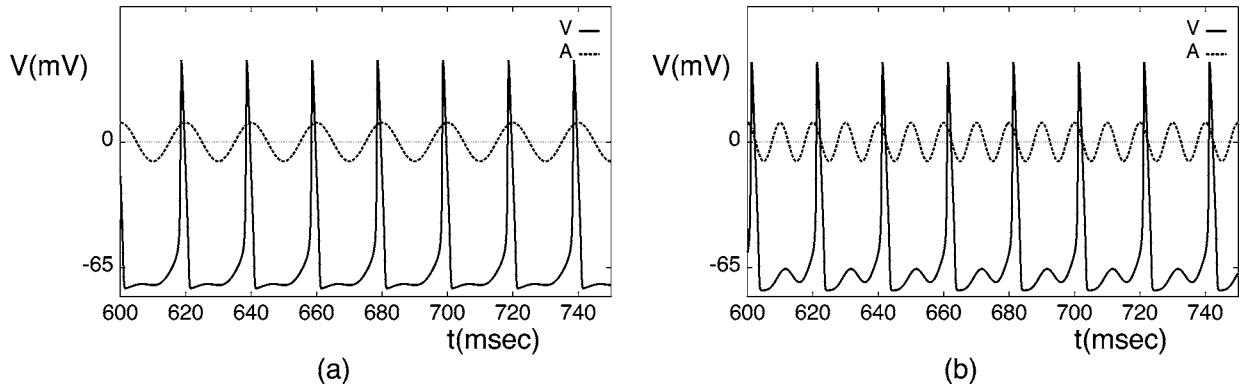

FIG. 1. The membrane potential responses of a Hodgkin-Huxley neuron under external sinusoidal current with $A=5\ \mu\mathrm{A/cm}^2$ and (a) $\omega=50$ Hz and (b) $\omega=100$ Hz. The profile of the sinusoidal currents is also plotted as dotted curves in the same figure.

FitzHugh-Nagumo neuron [20]. In these studies, the mode-locking structures in these systems construct Arnold tongue and bifurcations of the phase boundaries are identified. Our study of the bifurcation analysis in the Hodgkin-Huxley neuron can provide a canonical bifurcation structure for these simplified neural systems under periodic forcing.

This paper is organized as follows. The Hodgkin-Huxley neuron under sinusoidal current is introduced in Sec. II and order parameter analysis in Sec. III. The bifurcation analysis of the phase boundaries is performed in Sec. IV. The detailed analysis near selected areas in the phase diagram is done in Sec. V. Finally, the meanings and possible applications are discussed.

II. HODGKIN-HUXLEY EQUATION

The Hodgkin-Huxley neuron, which was first derived as a model of the squid giant axon [21], shows typical dynamics of a real neuron, the spiking behavior and the refractory period after a spike, and serves as a paradigm for the spiking neuron models based on nonlinear conductances of ion channels. A set of four coupled nonlinear ordinary differential equations in Hodgkin-Huxley neurons describes the dynamics of action potential generation involving four fundamental neurodynamic variables of V, m, n, and h. V is the membrane potential which represents the electric potential across the neural cell membrane, and m, n, and h are the gating variables for the ion channels through which ions cross and produce neural currents:

$$\frac{dV}{dt} = I_{ext} - g_{Na}m^3h(V - V_{Na}) - g_K n^4(V - V_K) - g_l(V - V_l),$$

$$\frac{dm}{dt} = \frac{m_\infty(V) - m}{\tau_m(V)},$$

$$\frac{dh}{dt} = \frac{h_\infty(V) - h}{\tau_h(V)},$$

$$\frac{dn}{dt} = \frac{n_\infty(V) - n}{\tau_n(V)},$$

where I_{ext} is the external forcing current injected into the neuron for stimulation. The parameters g_{Na}, g_K, and g_l are the maximum conductances for the sodium, potassium, and leakage currents, respectively, and V_{Na}, V_K, and V_l are the corresponding reversal potentials. The functions $m_\infty(V)$, $h_\infty(V)$, and $n_\infty(V)$ and the characteristic times $\tau_m(V)$, $\tau_n(V)$, and $\tau_h(V)$ in milliseconds are given in Refs. [21–23]. The detailed parameter values for the Hodgkin-Huxley neuron can be found in Refs. [21–23].

In the numerical experiments, the sinusoidal current $I_{ext}=A\cos(2\pi\omega t)$ is applied. The range of the amplitude of the external current, A, is chosen to be $1\sim5\ \mu\mathrm{A/cm}^2$, and the range of the frequency ω, 10–200 Hz. A small amount of the sinusoidal current with a low frequency is chosen to explore the effect of the maximal interaction between the external periodic forcing and the internal natural frequency.

III. ORDER PARAMETER ANALYSIS

Two membrane potential responses of a Hodgkin-Huxley neuron under various stimuli are shown in Fig. 1. These neural responses correspond to mode-locked states, where the periods of the firings are locked to the period of the external stimuli in integer ratios. Figure 1(a) corresponds to the 1/1 mode-locking response and Fig. 1(b) to the 1/2 mode-locking response. To characterize the mode-locked responses, it is useful to measure the *firing rate*, which is defined as the average number of spikes per period of driving stimulus. The firing rate defined here plays the same role as the rotation number in a typical quasiperiodic problem of the circle map [24]. The firing rate is generally used as an important order parameter characterizing the dynamical states of the neural responses when the periodic stimulus is applied.

The Hodgkin-Huxley neuron is capable of showing chaotic dynamics under periodic stimuli due to its highly nonlinear nature of the ionic conductances. The chaotic dynamics is characterized by the largest Lyapunov exponent, which measures the average rate of the exponential

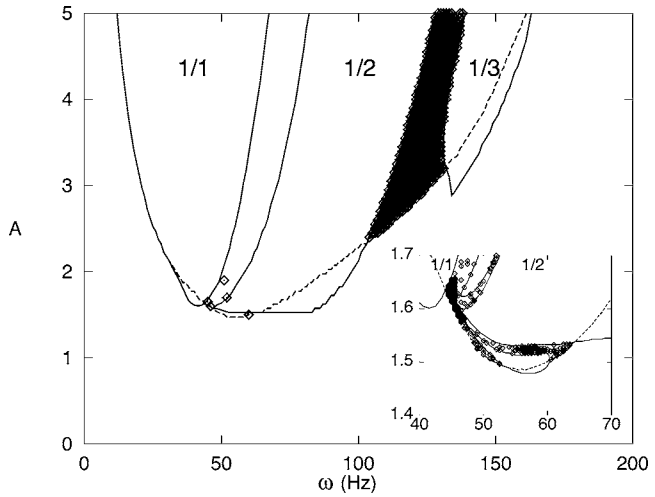

FIG. 2. Phase diagram of the Hodgkin-Huxley neuron under sinusoidal stimuli in the parameter space of the forcing amplitude A and frequency ω. The phase boundaries of 1/1, 1/2, and 1/3 mode-locked states are represented by solid curves and those of nonfiring state by dotted curves. The chaotic states with positive Lyapunov exponent are denoted as diamonds. Inset: the detailed phase diagram near $\omega=50$ Hz and $A=1.5$ μA/cm^2.

separation of two infinitesimally separated orbits. Chaotic states are identified from the positiveness of the largest Lyapunov exponent. In this study, the Wolf algorithm is adopted for the computation of the largest Lyapunov exponent [25].

Using the numerically computed firing rate and the largest Lyapunov exponent, the dynamical states are labeled in the parameter space of the periodic stimuli in an automated fashion. In the automated scan in the parameter space of the sinusoidal amplitude and the sinusoidal frequency, the last state after numerical integration is used as an initial condition for the next integration step at the new parameter value. This enables the exploration of the region of the hysteresis systematically. The phase diagram in the parameter space of the forcing frequency and the forcing amplitude is numerically explored and is shown in Fig. 2. Rich dynamical states including various mode-locked states and chaotic responses are observed. In the figure, solid and dotted curves represent the phase boundaries of mode-locked states and nonfiring states, respectively, and diamonds the parameter values for chaotic states. The ratios n/m denote the mode-locked responses with two integers m and n.

For a fixed A, the dependence of the firing rate as a function of the sinusoidal frequency ω gives a staircaselike structure which is similar to the devil's staircase in the typical quasiperiodic problem [26]. Each step in the staircase represents the same *rational* firing rate associated with the same qualitative dynamical state. For convenience, we call a state with a rational firing rate with n/m with integers m and n as the n/m *locked state* and the region in the parameter space with the same rational firing rate as the n/m *locked region*. Fundamental mode-locked regions with harmonic firing rates of $1/m$ with $m=1,2,3$ constitute the largest part of the mode-locked plateaus as in Fig. 2, which is qualitatively the same as the experimental results [5]. Nonfiring states without action potentials lie outside the mode-locking structure below the U-shaped firing onset curve. A relatively large region with hysteresis, which is enclosed by solid curves and dotted curves in Fig. 2, is also observed due to the bistability between the mode-locked states and the nonfiring state [5]. Note that the Hodgkin-Huxley neuron under the sinusoidal stimulus can start to fire at a much smaller threshold of 1.5 μA/cm^2 than that under a constant current of about 9.8 μA/cm^2 due to the resonance between the natural frequency and the external forcing frequency [27].

IV. OVERALL BIFURCATION STRUCTURE

The dynamical properties of mode-locked states and chaotic states near phase boundaries are analyzed through the "Poincaré section." The Poincaré section for the flow in the periodically stimulated system is a hypersurface in the phase space at a specified phase of the stimulus. The Poincaré map or the first return map is a mapping from one intersection of the trajectory to the next on the Poincaré surface of section. In this case, we take stroboscopic snapshots of the trajectory $\vec{x}(t)$ at time $t=nT$, $n=0,1,2,\ldots$, where $T=2\pi/\omega$. Then the Poincaré map P is defined by $\vec{x}((n+1)t)=P(\vec{x}(nt))$ and kth return map $P_{(k)}$ is given by $P_{(k)}=\overbrace{P\circ\cdots\circ P}^{k\ times}$. Mode-locked states correspond to fixed points in the return map, whose stability can be studied with the help of the stability analysis. Within mode-locked regions or the nonfiring region, the dynamical structure of trajectories or fixed points in the Poincaré map does not change as parameters are varied. At the phase boundaries, the dynamical structure of the trajectories changes qualitatively and the system goes through "bifurcations." The bifurcations at the phase boundary are investigated through bifurcation analysis of the Poincaré return map. This bifurcation analysis helps us to understand the instability mechanism of the stable fixed points in the Poincaré section and identify bifurcation types of phase boundaries. The numerical computation of bifurcation curves with continuation algorithms reveals detailed bifurcation structures for the phase boundaries.

The bifurcations at the phase boundary of the nonfiring state occur in three different types: the "inverse flip (IF) bifurcation," the "period-doubling (PD) bifurcation," and the "saddle-node (SN) bifurcation." In the case of the SN bifurcation, or the fold bifurcation, the stable fixed point disappears through pair annihilation with an unstable fixed point as the forcing amplitude is increased as in Fig. 3(a). One of the eigenvalues in the saddle-node bifurcation becomes +1 at the bifurcation point. In the case of the IF bifurcation, or the subcritical flip bifurcation, the stable fixed point changes its stability and becomes unstable when it meets the period-doubled unstable fixed points as in Fig. 3(b). One of the eigenvalues for this bifurcation becomes −1 at the bifurcation point. In this case, the bifurcation diagram shows a cascade of period-doubling bifurcations, eventually losing its stability at the end of the cascade as in Fig. 3(c).

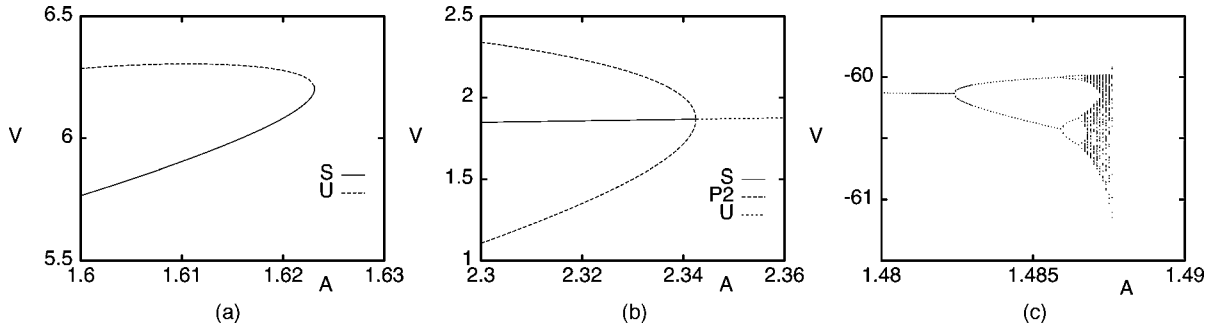

FIG. 3. Bifurcation diagrams in the map at the phase boundary of nonfiring region. (a) Saddle-node (SN) bifurcation at $\omega=44.5$ Hz and (b) inverse flip (IF) bifurcation at $\omega=103$ Hz and (c) the period doubling (PD) cascade at $\omega=55$ Hz. S, U, and $P2$ are the stable fixed point, unstable fixed point, and period-doubled unstable fixed point, respectively.

The numerical determination of the complex bifurcations has been done with the help of the continuation algorithms for the three types of bifurcations found in Fig. 4. The bifurcation curves in Fig. 4 are found to match the phase boundaries obtained from the order parameter analysis in Fig. 2. We find that in the phase diagram each phase boundary is composed of more than two types of bifurcations. Thus, at some points on the phase boundary the bifurcation type should change, which correspond to the codimension-2 bifurcation points. We find that three types of codimension-2 bifurcation points are commonly involved in organizing clusters of bifurcation curves in the phase diagram. In particular, we focus on the vicinity of four special points near the firing onset. The transitions from the SN bifurcation to the PD bifurcation are denoted as diamonds, those from the SN bifurcation to the IF bifurcation as rectangles, and those from the PD bifurcation to the IF bifurcation as circles in Fig. 4. The detailed bifurcation structures around these points in the phase diagram are investigated in detail with the bifurcation analysis and the continuation algorithm, which reveal myriads of underlying bifurcations.

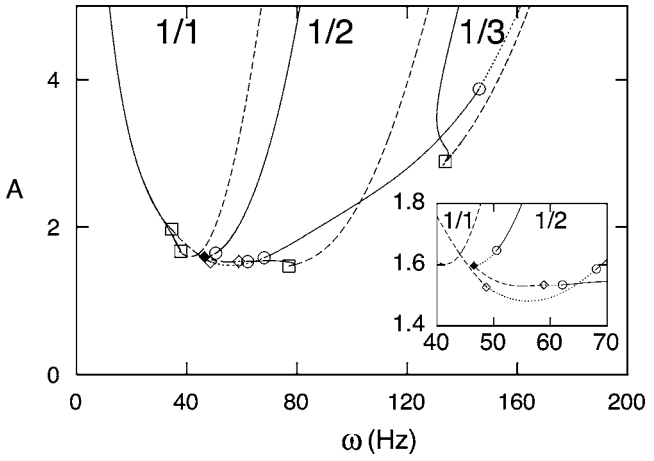

FIG. 4. Plot of the bifurcation types on the phase boundaries. Solid curves represent IF bifurcations, dotted curves the PD cascades, and dashed curves the SN bifurcations, respectively. The symbols represent the special phase points where the transition of bifurcations is at the phase boundary. Rectangles represent the transition from SN to IF bifurcations, open diamonds the transition from PD to SN, and circles the transition from PD to IF bifurcation, a solid diamond at $f\sim46$ Hz another type of transition from PD to SN bifurcation. Inset: the detailed phase diagram near $\omega=50$ Hz and $A=1.5$ μA/cm^2.

V. DETAILED BIFURCATION ANALYSIS

The typical bifurcation structure around the special points in the phase diagram denoted by open diamonds in Fig. 4 are investigated in detail and presented in Fig. 5(a), which corresponds to the phase boundary of the nonfiring state near $\omega=50$ Hz. As the forcing amplitude increases, the nonfiring state loses its stability through the PD cascade for $\omega>49$ Hz or the SN bifurcation for $\omega<49$ Hz. This SN bifurcation structure is created at $\omega=49.6$ Hz through the codimension-2 cusp singularity involving a pair creation of two SN bifurcation curves. The bifurcation curves of the PD cascade accumulate to one of the SN bifurcation curves. In these cases, the bifurcation type of the phase boundary appears to change from the PD cascade to the SN bifurcation around $\omega\sim49$ Hz. Detailed bifurcation diagrams are shown in Figs. 5(b)–5(d). Here, only the stable states are described for simplicity. The bifurcation of the phase boundary in Fig. 5(b) is of the SN type and that in Figs. 5(c) and 5(d) is of the PD type. Interestingly, there are two SN bifurcations in Figs. 5(b) and 5(c) and they separate the stable nonfiring state into two parts. A small stable part is labeled as S in Figs. 5(b) and 5(c).

The typical bifurcation structure around the phase points represented by circles in Fig. 4 is shown in Fig. 6(a), in particular close to the phase boundary of the nonfiring state near $\omega=66$ Hz. The nonfiring state loses its stability through the PD cascade when $\omega<67.8$ Hz or through the IF bifurcation when $\omega>67.8$ Hz. This transition occurs when the IF bifurcation curve meet the curve of the end of PD cascade. This IF bifurcation curve is created at $\omega\sim65$ Hz through a codimension-2 bifurcation; a PD bifurcation curve disappears, and IF and SN bifurcation curves are created instead. The bifurcation diagrams are shown in Figs. 6(b)–6(d), where only the stable states are seen. The bifurcations in Figs. 6(b) and 6(c) correspond to the PD cascade; however, that in Fig. 6(d) corresponds to the IF bifurcation.

The bifurcation structures around the phase points represented by rectangles in Fig. 4 are shown in Fig. 7(a), in particular close to the phase boundary of the 1/2 mode-

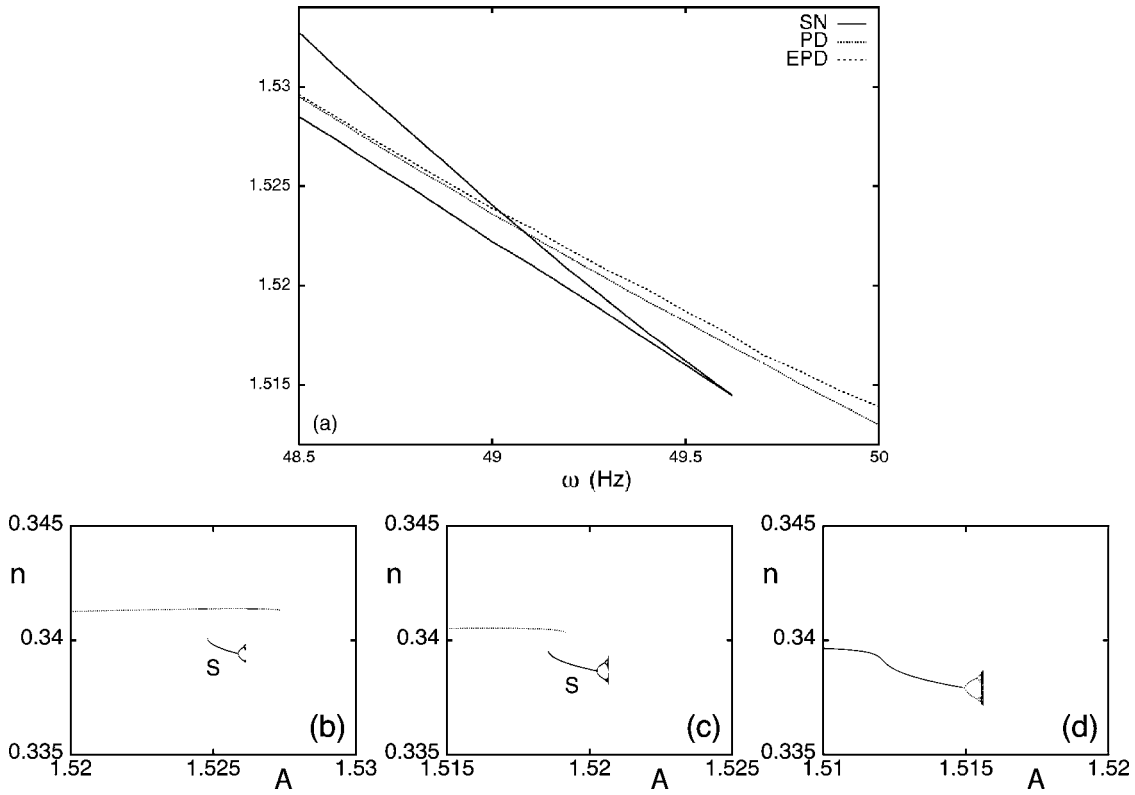

FIG. 5. Bifurcation structure of the phase boundary of the nonfiring state near ω=50 Hz. SN represents the saddle-node bifurcations, PD the PD bifurcation, and EPD the end of the PD cascade. The bifurcation diagrams of variable n at (b) ω=48.8 Hz, (c) ω=49.3 Hz, and (d) ω=49.8 Hz. S represents a strip of stable states.

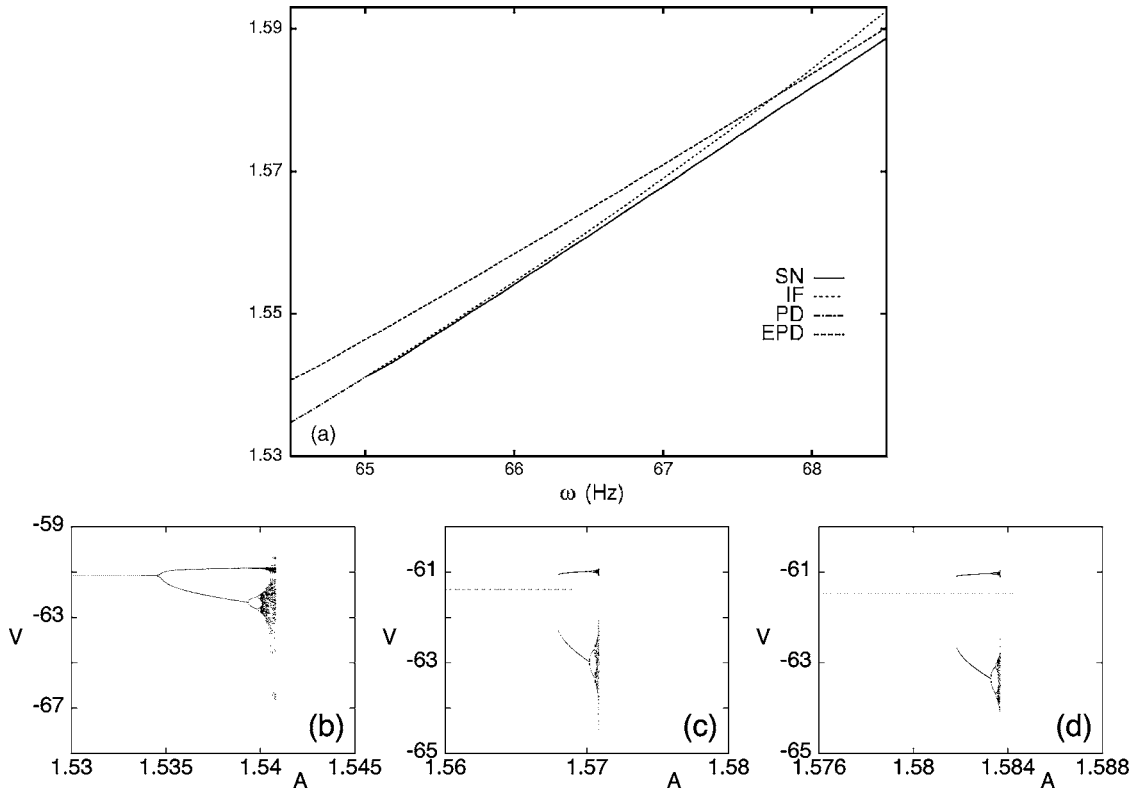

FIG. 6. Bifurcation structure of the phase boundary of the nonfiring state near ω=67 Hz. SN represents the saddle-node bifurcation, IF the inverse flip bifurcation, PD the PD bifurcation, and EPD the end of the PD cascade. The bifurcation diagrams at (b) ω=64.5 Hz, (c) ω=67 Hz, and (d) ω=68 Hz.

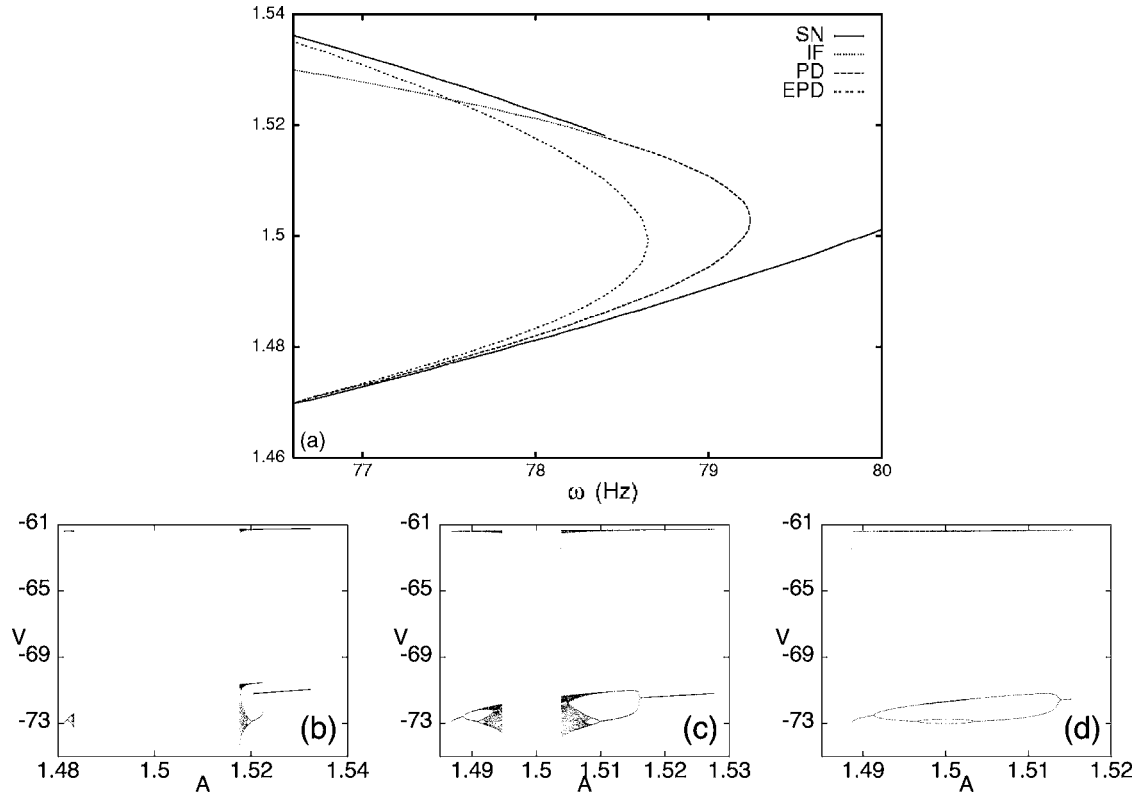

FIG. 7. Bifurcation structure of the phase boundary of the 1/2 mode-locked state near $\omega=79$ Hz. SN represents the saddle-node bifurcations, IF the inverse flip bifurcation, PD the PD bifurcation, and EPD the end of the PD cascade. The bifurcation diagrams at (b) $\omega=78$ Hz, (c) $\omega=78.6$ Hz, and (d) $\omega=78.8$ Hz.

locked state at $\omega=79$ Hz. The 1/2 mode-locked state loses its stability by the SN bifurcations when $\omega>78.5$ Hz and by the PD cascade when $78.5>\omega>77.5$ Hz and the IF bifurcation when $\omega<77.5$ Hz as the forcing amplitude is decreased. The PD cascade is created from the cascade of bubbling bifurcations, which correspond to a pair of PD bifurcations connected in the middle. In Fig. 7(a), the period-4 state is created from the stable period-2 state by the first bubbling bifurcation when $\omega\sim79.24$ Hz and the period-8 state by the second bubbling bifurcation at much smaller frequency [see Fig. 7(d)]. The stable states with longer periods are created successively through the sequence of bubbling bifurcations and eventually are connected as a pair of PD cascades. This sequence of bubbling bifurcations is shown in the bifurcation diagrams in Figs. 7(c) and 7(d). Here, only the stable states are presented for simplicity. The IF bifurcation curve created near $\omega=78.4$ Hz through a codimension-2 bifurcation of the first PD bifurcation curve disappears and IF and SN bifurcation curves are created instead. The effect of the codimension-2 bifurcation can be seen in the bifurcation diagrams in Figs. 7(b) and 7(c). The bifurcation type of the phase boundary becomes the IF bifurcation when it meets the curve of the end of the PD cascade near $\omega\sim77.5$ Hz.

There is another type of a special phase point represented by a solid diamond in Fig. 4. This bifurcation structure is found around the edge of the phase boundary of the 1/2 mode-locked state near $\omega\sim46$ Hz. This bifurcation structure involves a "swallow tail," a codimension-3 phenomenon consisting of the simultaneous creations of two pairs of cusp singularities for SN bifurcations. The PD bifurcation curves accumulate on one of the SN bifurcation curves. Around the swallow tail near the frequency $\omega\sim46.8$ Hz, the chaotic attractor in the PD cascade suddenly loses its stability when it encounters an unstable fixed point as in Fig. 8(b). Then the dynamics jumps to the stable fixed point. This interesting dynamical phenomenon is called the "boundary crisis." This chaotic attractor becomes stable again when the unstable fixed point disappears through the inverse SN bifurcation near $A\sim1.5988$ $\mu A/cm^2$.

In all these bifurcation diagrams, there appear strips of stable states, which have a PD cascade at one end and a SN bifurcation at the other end. You can see an example of the strips labeled by S in Figs. 5(b) and 5(c). Interestingly, the length of the cascade becomes shorter at smaller forcing frequency [compare Figs. 5(b) and 5(c)]. The instability mechanisms of the strip of stable states are investigated at the sufficiently small frequency of $\omega=46.75$ Hz as in Fig. 9(a). At this frequency, the PD cascade is shortened so much that the fixed points with higher periods are always unstable. Therefore, the stability of the period-1 fixed point becomes most important in the stability analysis. The occurrence of a very short branch of the stable fixed point is observed near the SN bifurcation as denoted by the solid line in Fig. 9(a) (labeled as B). The other branches of the fixed point are found to be unstable. At the end of stable fixed points, a new dynamical state of quasiperiodic oscillations labeled as Q is observed as in Fig. 9(a), which is created by the Hopf bifurcation involving a loss of the stability of the fixed point at

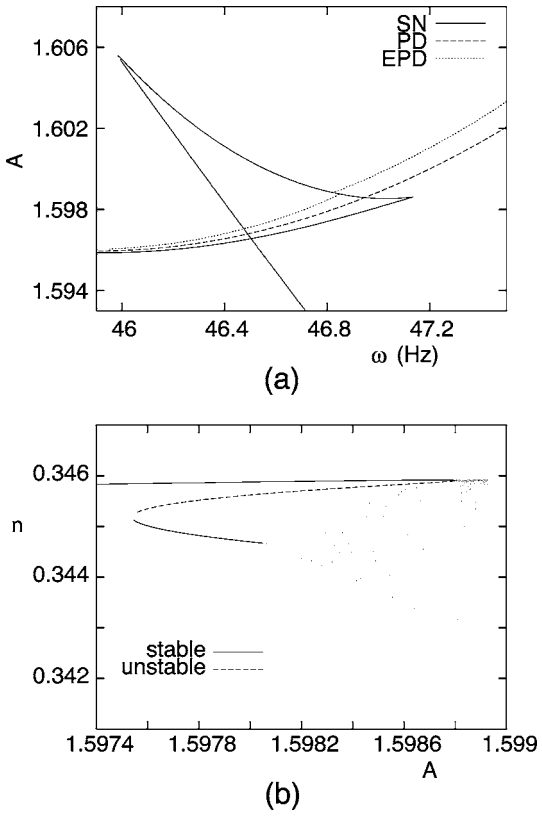

FIG. 8. (a) Bifurcation structure of the phase boundary of the 1/2 mode-locked state near $\omega=46$ Hz. SN represents the saddle-node bifurcation, PD the PD bifurcation, and EPD the end of the PD cascade. (b) The bifurcation diagrams at $\omega=46.84$ Hz. The dashed curve represents the unstable fixed point and the others the stable states.

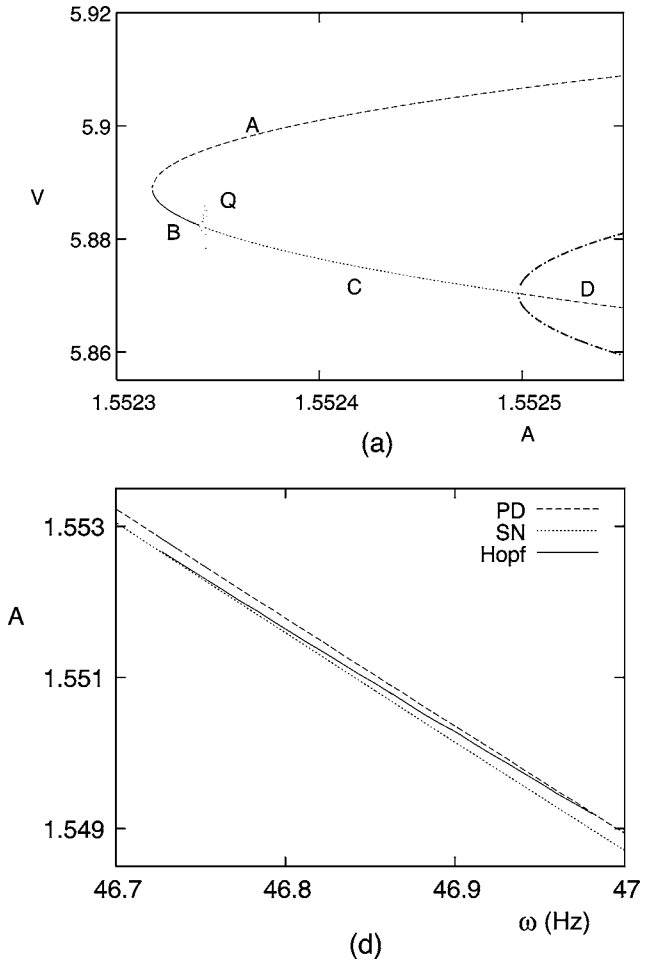

FIG. 9. (a) The bifurcation diagram of the phase boundary of the nonfiring state at $\omega=46.75$ Hz. The solid curve (B) represents stable fixed points, dashed curves (A and D) the unstable fixed points, dotted curve (C) the destabilized fixed points by Hopf bifurcation, two thick wavy curves at $A>1.5525$ μA/cm^2 and $V\leqslant 5.88$ μA/cm^2 the unstable period-doubled states, and Q the quasiperiodic state. (b) The bifurcation structure involving the Hopf bifurcation as a solid curve. The first PD bifurcation is denoted as a dashed curve, and the SN bifurcation is denoted as a dotted curve.

$A=1.552\,34$ μA/cm^2. The quasiperiodicity of a new dynamical state, which has two incommensurate frequencies, can be seen as a loop in the Poincaré section. For example, the bifurcation structure involving the Hopf bifurcation is shown in Fig. 9(b). The Hopf bifurcation curve meets the saddle-node bifurcation curve at A. A systematic study of the Hopf bifurcation will be necessary to complete the bifurcation picture involving quasiperiodic oscillations.

VI. SUMMARY AND DISCUSSION

The neural responses of the Hodgkin-Huxley neuron under sinusoidal forcing have been investigated with the help of a bifurcation analysis. The order parameters of the firing rate and the largest Lyapunov exponent give a rough sketch of the phase diagram for diverse dynamical states, which is qualitatively in agreement with those from neural experiments [5]. The complex bifurcation structures near firing onsets in the parameter space of forcing are explored in detail. In particular, the instability mechanisms of the phase boundaries of fundamental mode-locked states and nonfiring states have been studied through the bifurcation analysis around codimension-2 bifurcation points, which organize clusters of bifurcations including inverse-flip, period-doubling, and saddle-node bifurcations. The bifurcation types are specified for these phase boundaries with the help of the continuation algorithm.

In this paper, the bifurcations are studied near the phase boundaries of the fundamental mode-locked state and the nonfiring state. Numerical studies show that the observed instability mechanisms are also found near phase boundaries of higher mode-locked states and, therefore, can be quite general. A natural question is if these instability mechanisms can be observed in other excitable systems under periodic forcing. A preliminary study of the FitzHugh-Nagumo neuron, which is one of the simplified neuron models with excitability, reveals the tongue-shaped mode-locking structure in the phase diagram, the hysteresis region between the firing and nonfiring states, and three types of routes to chaos, qualitatively similar to that of the Hodgkin-Huxley neuron [28]. These similarities suggest that the bifurcation analysis in this paper can be applied to a wider class of excitable

systems under periodic stimuli, including the FitzHugh-Nagumo neuron.

Recently, the neurons under periodic forcing have been widely studied in the context of neuroinformation processing. These studies found various mode-locked states and quasiperiodic states which form Arnold tongues and other bifurcation structures in the phase diagram. Theoretical studies such as the bifurcation analysis focused on the integrate-and-fire neurons and the relaxation oscillators, which are simplified models of neurons. In contrast with these simple models, the Hodgkin-Huxley neuron under periodic forcing shows richer dynamics including hysteresis regions and complex bifurcation structures because of its nonlinearity in the conduction of ion channels and the rigidity of the natural frequencies. The bifurcation analysis of the Hodgkin-Huxley neuron can provide a canonical bifurcation structure for typical spiking neurons with refractory periods, which can contribute to the understanding of neurosignal processing in real neurons.

ACKNOWLEDGMENTS

We would like to thank W. G. Choe for stimulating discussions and helpful comments. This work was supported by the Brain Research Project and by a grant from the MOST/KOSEF to the National Core Research Center for Systems BioDynamics (No. R15-2004-033).

[1] A. Brandstäter, J. Swift, H. L. Swinney, A. Wolf, J. D. Farmer, E. Jen, and J. P. Crutchfield, Phys. Rev. Lett. **51**, 1442 (1983); S. Martin, H. Leber, and W. Martienssen, *ibid.* **53**, 303 (1984); P. Bak and M. H. Jensen, Phys. Scr. **T9**, 50 (1985); M. H. Jensen, P. Bak, and T. Bohr, Phys. Rev. A **30**, 1960 (1984).
[2] H. G. Schuster, *Deterministic Chaos* (VCH, Weinheim, 1989).
[3] K. Aihara and G. Matsumoto, in *Chaos in Biological Systems*, edited by H. Degn, A. V. Holden, and L. F. Olsen (Plenum, New York, 1987); K. Aihara, T. Numajiri, G. Matsumoto, and M. Kotani, Phys. Lett. A **116**, 313 (1986).
[4] G. Matsumoto, K. Aihara, Y. Hanyu, N. Takahashi, S. Yoshizawa, and J. Nagumo, Phys. Lett. A **123**, 162 (1987); K. Shimokawa, Y. Hanyu, and G. Matsumoto, J. Phys. Soc. Jpn. **67**, 2534 (1998).
[5] N. Takahashi, Y. Hanyu, T. Musha, R. Kubo, and G. Matsumoto, Physica D **43**, 318 (1990).
[6] P. Arrigo, L. Marconi, G. Morgavi, S. Ridella, C. Rolando, and F. Scalia, in *Chaos in Biological Systems*, edited by H. Degn, A. V. Holden, and L. F. Olsen (Plenum, New York, 1987).
[7] S. G. Lee and S. Kim, Phys. Rev. E **60**, 826 (1999).
[8] J. P. Baltanas and J. M. Casado, Phys. Rev. E **65**, 041915 (2002).
[9] C. R. Laing and A. Longtin, Phys. Rev. E **67**, 051928 (2003).
[10] Y. Jiang, Phys. Rev. E **71**, 057103 (2006).
[11] M. R. Guevara, A. Shrier, and L. Glass, Am. J. Physiol. **254**, H1 (1988).
[12] P. H. E. Tiesinga, P. Thomas, J.-M. Fellous, and T. Sejnowski, Abstr. Soc. Neurosci. **27**, 821.12 (2001).
[13] P. H. E. Tiesinga, Phys. Rev. E **65**, 041913 (2002).
[14] A. V. Holden, Biol. Cybern. **21**, 1 (1976).
[15] D. MacKay and W. MaCulloch, Bull. Math. Biophys. **14**, 127 (1952).
[16] S. Sato and S. Doi, J. Math. Biol. **112**, 243 (1992); S. Goshen, A. Rabinovitch, and R. Thieberger, J. Theor. Biol. **160**, 179 (1993); T. Nomura, S. Sato, J. P. Segundo, and M. D. Stiber, Jpn. J. Health Phys. **72**, 55 (1994); S. Doi and S. Sato, J. Math. Biol. **125**, 229 (1995).
[17] J. Stoer and R. Bulirsch, *Introduction to Numerical Analysis* (Springer-Verlag, New York, 1991).
[18] Y. A. Kuznetsov, *Elements of Applied Bifurcation Theory* (Springer, New York, 1998).
[19] S. Coombes and P. C. Bressloff, Phys. Rev. E **60**, 2086 (1999); S. Coombes and A. H. Osbaldestin, *ibid.* **62**, 4057 (2000); S. Coombes, M. R. Owen, and G. D. Smith, *ibid.* **64**, 041914 (2001).
[20] A. D. Garbo, M. Barbi, and S. Chillemi, Int. J. Bifurcation Chaos Appl. Sci. Eng. **11**, 2549 (2001).
[21] A. L. Hodgkin and A. F. Huxley, J. Physiol. (London) **117**, 500 (1952).
[22] S. G. Lee, S. Kim, and H. Kook, Int. J. Bifurcation Chaos Appl. Sci. Eng. **7**, 889 (1997).
[23] D. Hansel, G. Mato, and C. Meunier, Europhys. Lett. **23**, 367 (1993).
[24] S. Ostlund, D. Rand, J. Sethna, and E. D. Siggia, Physica D **8**, 303 (1983).
[25] A. Wolf, J. B. Swift, H. L. Swinney, and J. A. Vastano, Physica D **16**, 285 (1985).
[26] P. Bak, Phys. Today **39**(12), 38 (1986).
[27] S. G. Lee, Ph.D. thesis, Pohang University of Science & Technology (POSTECH), 1999.
[28] S. G. Lee and S. Kim (unpublished).